Correlation between the microstructure of carbon materials and their potassium ion storage performance

Xiuyi Lin[†, a], Jiaqiang Huang[†, a], and Biao Zhang[a,b]*

aDepartment of Applied Physics, The Hong Kong Polytechnic University, Hung Hom, Hong Kong, P.R. China.
bThe Hong Kong Polytechnic University Shenzhen Research Institute, Shenzhen, P.R. China

Abstract

Alkali-metal ions storage in carbon materials is of great interests for developing high performance anodes for batteries. While Li, Na ions storage has been extensively investigated, systematic studies on the correlation between K ions storage and carbon microstructure have rarely been conducted. The large radius of K ions leaves a legitimate question whether the charge storage sites for Li and Na ions are also active for K ions. Herein, electrospun carbon nanofibers are employed as model materials to explore the K-ion storage behaviors in carbon with representative microstructures. By combining in-situ characterization and theoretical calculations, three active sites have been unveiled, including: (i) uptake of K-ion by defect sites; (ii) K ions adsorption on isolated graphene sheets in partially disordered carbon; (iii) K ions intercalation between graphene layers for carbon with a high degree of graphitization. A similar reversible capacity around 280 mAh/g is obtained for various carbon structures while their voltage profiles are highly disparate. Remarkably, it is found that non-graphitic carbon presents better rate capability and less temperature-dependence due to the faster ion diffusion. These findings offer new insights into the design of advanced carbon anode materials with tunable properties for K-ion batteries

Keywords: carbon, anodes, in-situ characterization, K-ion batteries

1. Introduction

The ever-increasing demand for Li-ion batteries has raised concern on the depletion of lithium sources. A merely 20 ppm of lithium in the earth crust leaves a question whether Li-ion batteries could afford the future large-scale application [1]. Research on Na-ion and K-ion batteries have been therefore revived since the 2010s for the consideration of sustainable development. Thanks to the abundance of sodium and potassium in nature, a much-reduced cost

*Corresponding author: Tel: (+852) 34003260. Email address: biao.ap.zhang@polyu.edu.hk (Biao Zhang)

is expected for Na- and K- ion batteries, thus making them promising candidates for stationary energy storage [2,3]. Recent studies on K-ion batteries delightedly show that several cathode materials like Prussian blue $K_xMnFe(CN)_6$ [4,5], layered oxides $K_{0.7}(FeMn)_{0.5}O_2$ [6], and polyanionic $KVPO_4F$ [7] are capable of delivering comparable capacities with their counterparts in Li/Na- ion batteries. On the anode sides, it is well known that the intercalation of potassium ions into graphite and some metal oxides could be readily achieved at a moderate voltage [8–11]. These findings clearly indicate the possibility of building a K-ion battery with decent performance.

Through the formation of stage I graphite intercalation compound (GIC) in the form of KC_8, graphite possesses a theoretical capacity of 279 mAh/g [12]. Although a practical capacity of 200-230 mAh/g after 100 cycles has been reported [8,13,14], still falling far behind ~350 mAh/g for lithium storage. Therefore, extensive studies have been conducted in the quest of high-performance carbon anode for K-ion batteries, including modification of microstructure [15,16], doping of the heteroatoms [14,17], and optimization of the electrolyte systems [13]. Previous studies on Li/Na storage suggest that carbon materials enjoy a variety of active sites through various mechanisms beyond intercalation [18–20]. Although alkali-metal ion storage in carbon materials share similarities in many aspects, a systematic investigation on potassium ion storage mechanism in carbons beyond intercalations is lacked. Exploring the additional active sites is hence eagerly desired for accelerating the design of better carbon anodes.

A systematically study is conducted in current work to tailor the atomic structure of carbon materials and to examine their potassium ion storage behavior, based on which the correlation between the microstructure and electrochemical performance is established. A self-sustained carbon nanofiber (CNF) film is employed as a model material to avoid the influence of binder and conductive additives that used in conventional electrodes. The CNF films are produced by electrospinning using polyacrylonitrile (PAN) as the precursor, followed by stabilization and carbonization to transform PAN into carbon. The carbonization temperature was gently controlled to gradually tune the functionality and to increase the ordered structure of CNFs, thus allowing the detailed investigation of potassium ion storage in carbon materials with various composition and microstructure.

2

2. Experimental

2.1 CNFs Preparation and characterization

CNF films were fabricated by electrospinning, a typical process is dissolving 5 wt% PAN (Sigma, Mw of 150,000) in N-dimethylformamide and stirring for 12 h. Then the PAN solution was electrospun into fiber shape under a high voltage of 13 kV at a feed rate of 1.0 mL/h using a needle of diameter 1.2 mm. The PAN fiber film was collected on an Al foil and peeled off after drying. Then the film was stabilized at 250 °C for 3 h in a muffle furnace to achieve a cyclic structure and hence avoid the melting of PAN during high-temperature treatment. The carbonization was conducted by treating the stabilized films under Ar atmosphere for 1 h at 650, 1250, and 2800 °C, and the corresponding samples are denoted as CNF-650, CNF-1250, and CNF-2800, respectively. The morphologies of CNFs were examined using TEM (JEOL 2010F) and SEM (JEOL-6490). The crystal structure was studied using Witec Confocal Raman system with a 532nm laser. CNFs surface functionality was assessed by XPS (PHI5600, Physical Electronics, Inc.) spectrometer using an Al Kα monochromatic source (14 kV).

2.2 Electrochemical Tests

Free-standing CNF films were used directly as electrodes in 2032 coin cells, where a K metal was used as counter electrode. 1M KPF_6 in ethyl carbonate (EC)/dimethyl carbonate (DMC) (1:1 by volume) and glass fiber (Whatman, GF/D) were employed as the electrolyte and separator, respectively. The coin cells were charge/discharge cycled at different current densities between 0 and 3 V on a LAND 2001 CT battery tester. Electrochemical impedance spectroscopy (EIS) was carried out on a VMP system (Biologic S.A., Claix, France). During the in-situ Raman test, the cyclic voltammetry (CV) scan was conducted using an electrochemical workstation (ZAHNER-elektrik GmbH & Co.) with a sweep rate of 0.5, 1, 2 and 4 mV/s.

2.3 Theoretical Calculations

The project augmented wave method [21] implemented in the Vienna Ab initio Simulation Package [22] with the generalized gradient approximation as parameterized by Perdew-Burke-Ernzerhof [23] was used to perform the DFT calculations. The vdW-optPBE correction method was utilized to correctly describe the van der Waals interactions [24]. Spin polarization was also considered. An energy cutoff of 500 eV was chosen. A spacing less than 0.05 $Å^{-1}$ was used to

sample the Brillouin zone including the gamma point. The convergence criteria were 10^{-6} eV and 0.02 eV Å^{-1} for the energies and forces, respectively.

3. Results and Discussion

According to previous studies, there are three regimes during the transformation of polymer precursors to graphitic carbon [25,26], as indicated in Fig. 1. Below the temperature of 1000 °C, the formation of C-C aromatic structures occurs accompanied by the elimination of impurities. These small C-C islands gradually grow with increasing temperature above 1000 °C, leading to the appearance of graphene domains, which are randomly located throughout the material. The isolated graphene sheets start to rotate to be orientated in the basal plane at a super-high temperature over 2000 °C. Together with the further growth of the domain size, a graphite-like structure is constructed while the graphitization degree varies with the nature of precursors. The structure evolution of CNFs annealed under different temperatures is confirmed by the Fourier-transform infrared spectroscopy (FTIR) spectra (Fig. S1) and transmission electron microscopy (TEM) images as discussed later. In order to explore the correlation between the carbon microstructure and K ion storage behaviors, three annealing temperatures, i.e., 650, 1250 and 2800 °C are selected to produce the carbon with disordered structure, partially ordered structure and ordered structure, respectively. The samples are denoted as CNF-x for conciseness where x represents the temperature. Changing the carbonization temperature does not affect much the fibrous morphology. The CNFs have diameters of 100-300 nm with "beads" free morphology as indicated by scanning electron microscope (SEM) (Fig. S2). With increasing carbonization temperature, the functional groups in CNFs are removed leaving a dense package, thus the diameter of CNFs is slightly reduced. To further explore the textural features of CNFs, the BET surface area and pore size distribution were assessed by nitrogen adsorption, as indicated in Fig. S3. The three samples have similar surface area of ~20 m^2/g with a pore volume of ~0.03 cm^3/g.
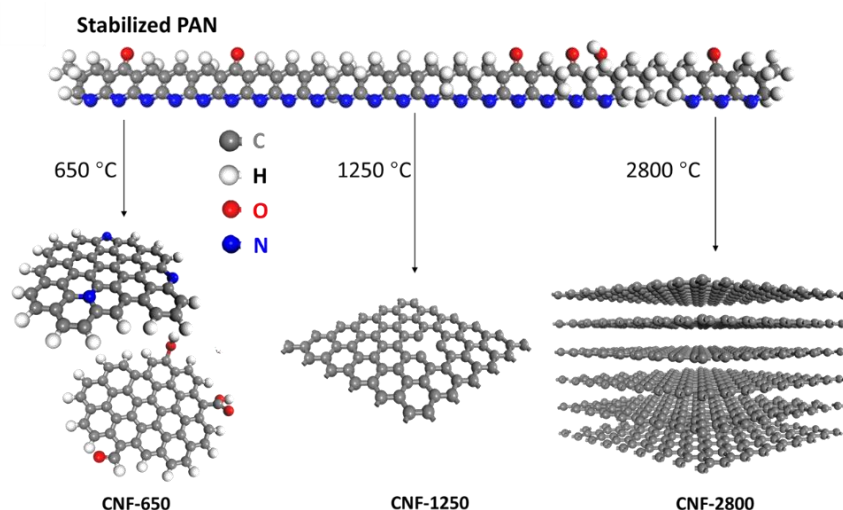
4

Fig. 1 Correlation between the microstructure of CNFs and the annealing temperature.

3.1 Correlation between K ion storage and microstructure

As expected, the low temperature of 650 °C is not enough to fully carbonize the CNFs. The TEM image of the sample shows a characteristic of amorphous carbon without apparently ordered texture (Fig. 2a). It is found that a high amount of N and O heteroatoms is left in CNF-650, giving a relatively low carbon content of only 79.7 at.%. The oxygen mainly comes from oxygenated functional groups such as –COOH, -C=O, revealed by the X-ray photoelectron spectroscopy (XPS) results (Fig. S4). These oxygen groups were introduced during stabilization process under air, where a ladder structure was constructed with the aid of oxygen. Turning to the nitrogen, several peaks are observed corresponding to graphitic-N (2.2 at.%), pyridinic-N (8.0 at.%), and pyrrolic-N (4.3 at.%) (Fig. 2b). The high N content originates from the PAN precursor which has a chemical formula of $(C_3H_3N)_n$. Superior amount of N is kept under the low carbonization temperature, yielding an *in-situ* N-doped carbon. Due to the chemical valence difference between C and N, the substitution of C by N induces plenty of defect sites, which are considered active towards K ions.

The electrochemical performance was then tested versus K metal in 2032 coin cells. A large irreversible capacity was observed in the first cycle (Fig. 2e), which is attributed to the solid electrolyte interface (SEI) formation on the high-surface-area CNFs. Coulombic efficiencies rapidly increased in the following cycles as an indication of forming a stable electrode-electrolyte interface. The voltage profiles of CNF-650 do not show any clear plateaus but present

a monotonous decrease in the voltage. Such behaviors are reminiscent of the Li and Na ions storage in disordered carbon. Intercalation of alkali-metal ions is not possible in this type of carbon materials due to the lack of graphitic domains. Instead, functional groups and defects are able to host the ions according to previous studies on alkali-metal ion storage [14,25]. To confirm the assumption, a theoretical calculation based on density functional theory (DFT) is performed. The reaction potential is calculated as follows:

$$U = -\frac{E_{CK} - E_C - E_K}{e} \tag{1}$$

where U is the theoretical potential of the potassium adsorption on the defective graphene, ECK, EC, and EK are the DFT calculated ground-state energies of the potassium-adsorbed defective graphene, the defective graphene, and the potassium metal, respectively, and e is the elementary charge.

We first calculate the adsorption energy of K ions in N-induced defects. The results in Fig. 2d reveal that the theoretical potentials of K ions storage in graphitic-N, pyrrolic-N and pyridinic-N are 0.183 V, 1.439 V, and 1.342 V, respectively (all potentials are vs. K^+/K unless otherwise stressed). Oxygenated functional groups could also serve as redox centers for faradaic reactions. For instance, the carbonyl group (C=O) has been reported to be reduced by Li ions at a high voltage between 1.5 to 3.5 V vs. Li^+/Li which is reversible upon the oxidation [27,28]. A similar phenomenon is expected towards K ions: the calculation results demonstrate that the electrochemical reactions for –COH, -COOH, -C=O take place at 0.832 V, 1.682 V, and 1.771 V, respectively (Fig. 2c). This result shows a good agreement with the charge/discharge curves (Fig. 2e), where the large portion of the capacity is contributed from the potential higher than 0.5 V. It should be mentioned that the reaction potential would be affected by the concentration of the functional groups, thereby leading to the sloping features in the voltage profiles. As a control, the binding energies of protonated graphene were also calculated: -0.932 and -0.817 eV for the edge and plane sites (Fig. S5), respectively. It indicates that the binding of K ions can be enhanced by N-induced defects and oxygenated functional groups.
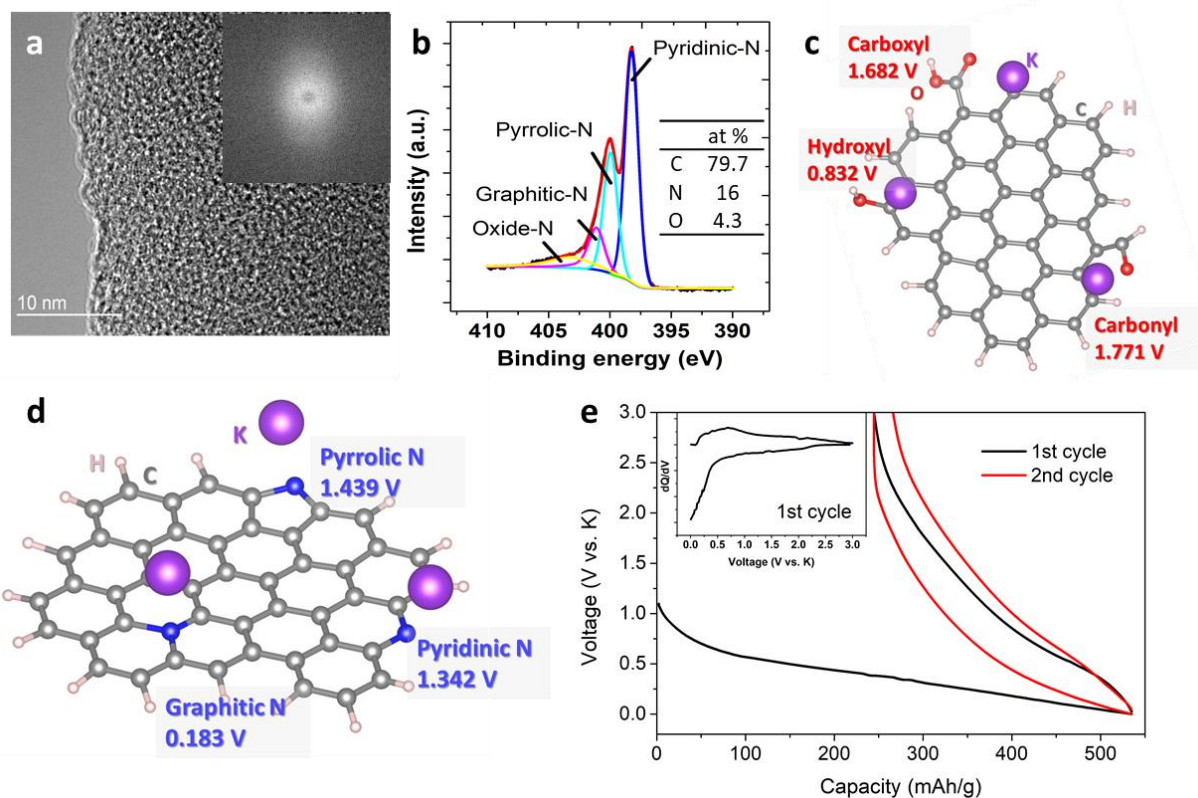
Fig. 2 (a) TEM image of CNF-650 (inset showing the FFT image); (b) Deconvoluted N1s spectra for CNF-650; Calculation results of adsorption energy of potassium ion on (c) N-doped graphene and (d) oxygenated functional groups; (e) Voltage profile of CNF-650 at the current density of 25 mA/g, inset is the dQ/dV plot.

The capacity contribution of the heteroatoms is further confirmed through the investigation of the samples annealed at a higher temperature. The N and O contents are considerably decreased when the carbonization temperature is increased to 1250 °C. The XPS results in Fig. 3b show that the C content is increased to 97.8 at.% with only 0.8 at.% N and 1.4 at.% O left. Consequently, almost all the capacity in the voltage profiles of CNF-1250 is located at the potential regime lower than 1 V, compared to over 60% of the total capacities come from 1-3 V in CNF-650. The calculation results have shown most of the reactions with N, and O related sites occur at a potential higher than 1 V. The removal of these heteroatoms would significantly decrease the capacities in the region. Nevertheless, CNF-1250 still delivers a reversible capacity of 250 mAh/g at a current density of 25 mA/g, close to that of CNF-650. It indicates the involvement of additional active sites to contribute extra capacities. The TEM (Fig. 3a) shows the appearance of average five layers graphene sheets in size of several nanometers, which are

7

the typical characteristics of carbon materials prepared between 1000 and 2000 °C. The low carbonization temperature could not provide sufficient energy to drive the graphitization, resulting in the absence of graphitic domains for the intercalation of K ions. This structure was proposed as "Card house" model by J. Dahn et al. previously, where the randomly oriented graphene sheets form a "house" to host the Li/Na ions [29]. In this way, the isolated graphene sheets possibly serve as active sites for the adsorption of K ions.

The capability of graphene sheets in housing K ions is proved by DFT calculation results (Fig. 3c), which predicts the adsorption begins at around 0.5 V. The derivative curve (dQ/dV) clearly shows an oxidation peak at 0.52 V (Fig. 3d and Fig. S6), in good agreement with the prediction. The adsorption potential decreases with the increasing K. Therefore, a sloping curve is observed instead of a flat plateau. When reaching a high concentration of K ions, the adsorption energy turns to be stabilized at around 0.15 V, which is responsible for the 0.2 V peak in dQ/dV curve. As one may still argue whether K ions intercalation occurs in this kind of partially ordered carbon, an *in-situ* Raman study was therefore conducted. Previous studies demonstrate that the G-band peak of carbon in Raman spectra could be used as an indicator to monitor the staging behavior during K ions intercalation [30,31]. The Raman spectrum of pristine CNF-1250 is like that of CNF-650 (Fig. S7 and S8) but with a more prominent G-band peak due to the growth of aromatic structure. The peak is well kept in the full charge/discharge cycle with neither evident broadening nor position shift (Fig. 3e). The *in-situ* XRD measurement (Fig. S9) also presents no obvious changes during the discharge/charge process, supporting the adsorption of K ions on the surface of graphene sheets instead of intercalation. The observation rules out the K ions intercalation in CNF-1250.
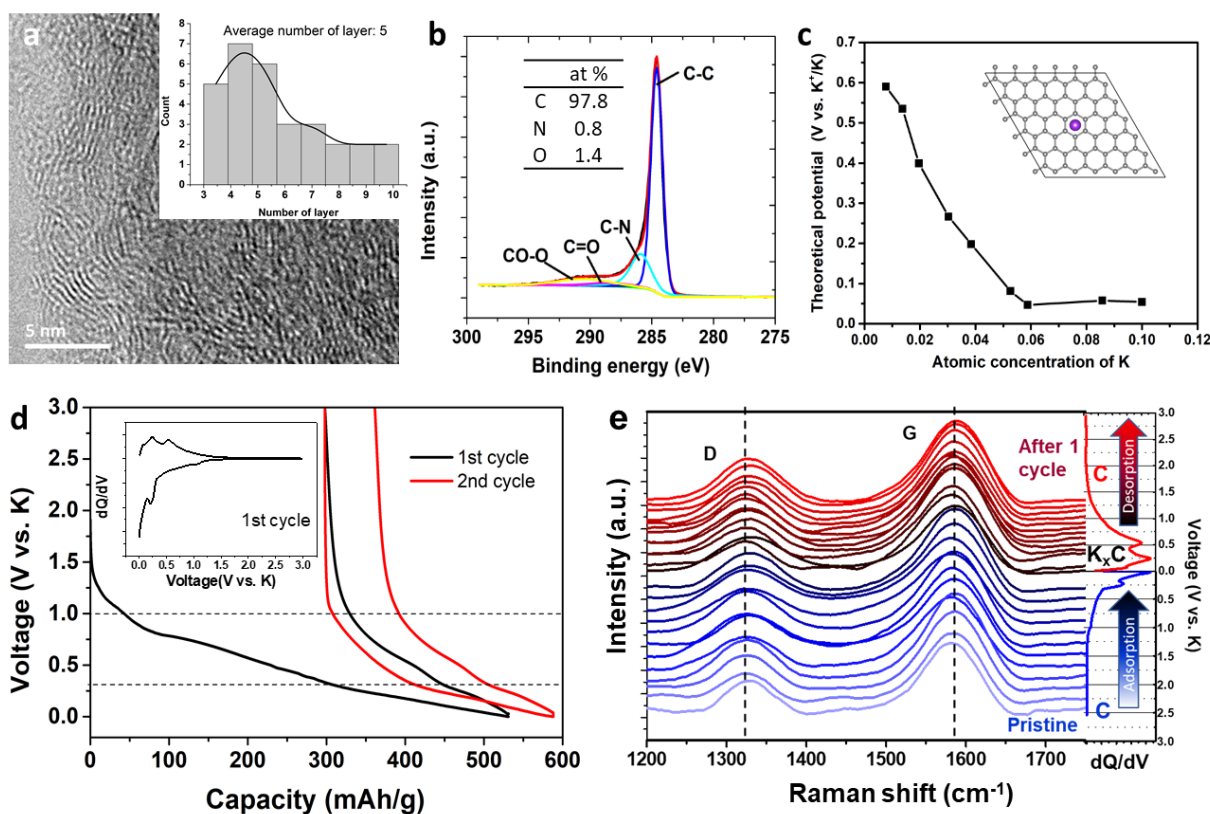
Fig. 3 Potassium ion storage in partially ordered carbon. (a) TEM image of CNF-1250; (b) Deconvoluted C 1s spectra for CNF-1250; (c) Comparison between theocratical reaction potentials of potassium ion on graphene sheet and the 2nd discharge curve; (d) Voltage profiles of CNF-1250 at the current density of 25 mA/g, inset is the dQ/dV plot; (e) Selective *in-situ* Raman spectra of CNF-1250 with corresponding dQ/dV plot.

To explore the K ions storage in graphitic carbon, a high annealing temperature of 2800 °C was employed to graphitize the CNFs. The appearance of 5-13 layers graphene is observed in TEM image (Fig. 4a), proving the formation of graphite-like domains, although with the presence of small disorder region. The graphitization degree is characterized by calculating the crystallite size (L_a) from the integrated intensities ratio of the D and G Raman bands, which is 40.2 nm for CNF-2800 and it is much larger than L_a of CNF-650 and -1250 (Fig. S8). Almost all the heteroatoms are removed under such high temperature, resulting in a nearly 100% carbon content as indicated in XPS result (Fig. S10). The voltage profiles of CNF-2800 show a cascade feature that closes to the curves of graphite (Fig. 4b and Fig. S11). A discharge plateau at 0.75 V corresponding to SEI formation is observed in the initial discharge which becomes inapparent in the subsequent cycles as the formation of SEI occurs mostly in the first cycle. The SEI formation potential is slightly different from those in CNF-650 and CNF-1250, suggesting the important

9

role of carbon microstructure in constructing stable SEI which deserves further studies. Following that, a sloping region between 0.5 and 0.2 V appears after which a plateau at 0.1 V shows up. *In-situ* Raman tests were conducted to real-time monitor the structural change in K ion intercalation as well (Fig. 4c). The pristine CNF-2800 presents a weak D band and a sharp 2D band, indicating the highly ordered structure. During the potassiation, the weakening of the D band is first observed at 0.75 V, and the peak is almost disappeared at 0.5 V, which coincides with the formation of the SEI layer [32]. The intensity of 2D band also steadily decreases with potential until finally vanished at 0.25 V. A similar loss of 2D band has previously been observed by Pint et. al., who pointed out that the 2D band is absent for stage I (KC_8) and stage II (KC_{24}) GICs but present for the higher order stages [33]. The 2D double resonance is the response to the inner uncharged graphite layers; when all graphite layers are charged with K, the double resonance is concealed for the outer charged layers. Hence the 2D band disappears as a result of K ions intercalation. From 0.25 to 0 V, a broadening band with asymmetric Breit-Wigner-Fano line-shape is observed around 1550 cm^{-1}, which confirms the formation of stage I GIC KC_8 [34].

As the graphene layers in CNF-2800 are not as well oriented as in graphite, the ions randomly inserted between all the graphene layers. Thus, only the downshift of G band is observed without splitting as reported in graphite. During the depotassiation, the G peak first shifts back by 0.25 V, then the 2D band restores at 0.55 V, and finally D band is partially recovered, indicating the reversibility of K insertion/extraction in CNF-2800. The results fully agree with the *in-situ* XRD tests, which show the appearance of GIC when discharged to 0 V followed by the recovery of carbon structure upon subsequent charging to 3 V (Fig. S9).
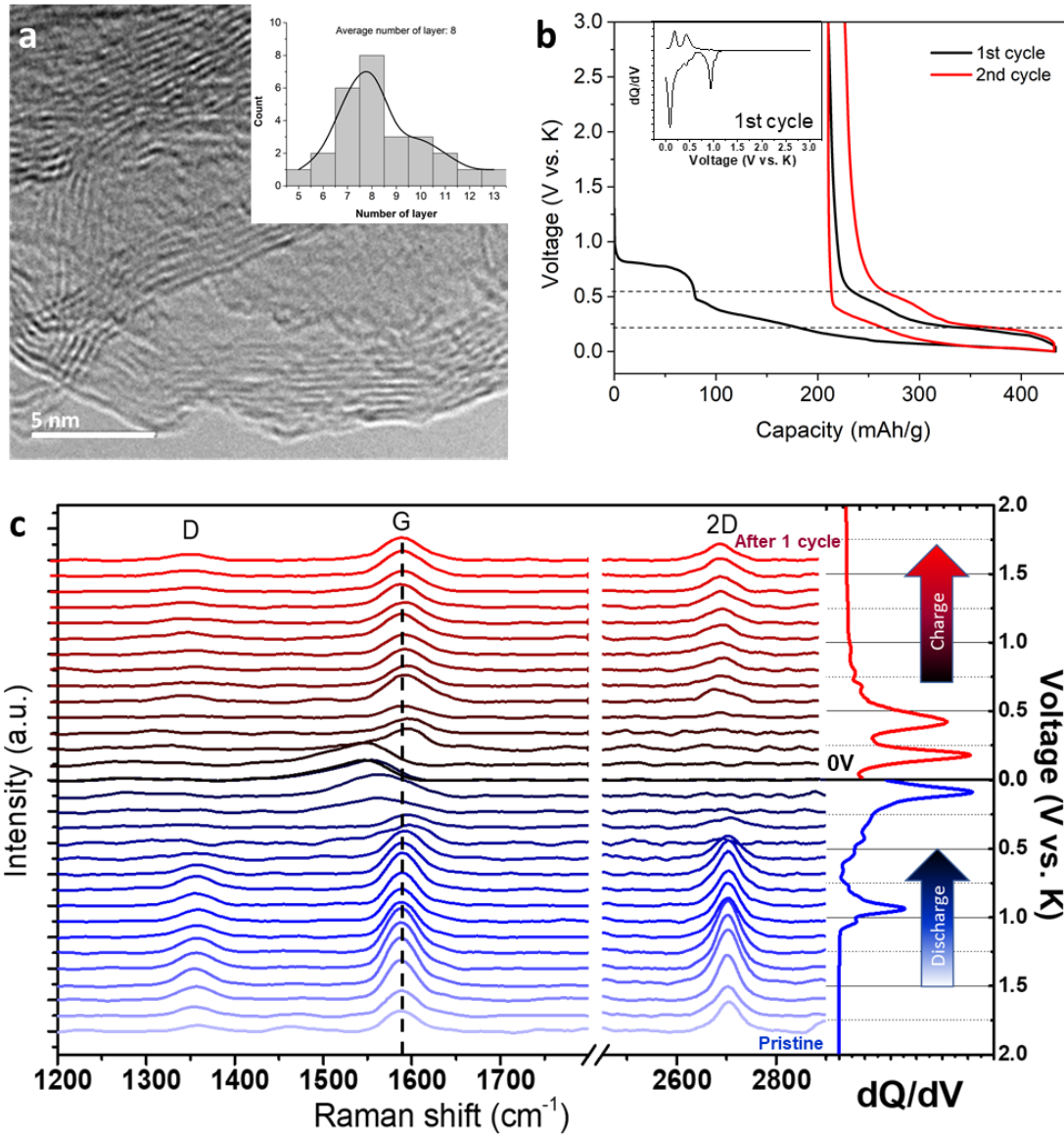
Fig. 4 Potassium ion storage in graphitized carbon. (a) TEM image of CNF-2800; (b) Voltage profile of CNF-2800 at the current density of 25 mA/g, inset is the dQ/dV plot; (c) Selective in-situ Raman spectra of CNF-2800 with corresponding dQ/dV plot

3.2 Effects of K-ion storage mechanism on the electrochemical performances

The K-ion storage behaviors were further characterized by the cyclic voltammetry test conducted at various scan rates. The data are fitted based on the following equation:

$$i = av^b \tag{2}$$

where i is the peak current, and v is the sweep rate. The value of b could be used as an indicator to distinguish the faradaic and capacitive contributions. A number of $b = 0.5$, i.e., i is

proportional to the square root of *v*, suggests the faradaic reaction, while the capacitive behavior has $b = 1$ (*i* is proportional to *v*). By fitting the plot of log(*i*) versus log(*v*), *b*-values are determined to be 0.77, 0.66 and 0.49 for CNF-650, CNF-1250 and CNF-2800, respectively (Fig. 5a). The results support the proposed mechanisms well. The charge storage in CNF-2800 only makes use of the intercalation-induced faradaic reaction. In comparison, significant surface capacitive contribution occurs in CNF-650 and CNF-1250. Furthermore, redox peaks of CNF-2800 become inapparent when the increasing the scan rate, while the effects of scan rate on CNF-1250 are less significant (Fig. S12). This also indicates the fast kinetics in CNF-1250 than in CNF-2800.
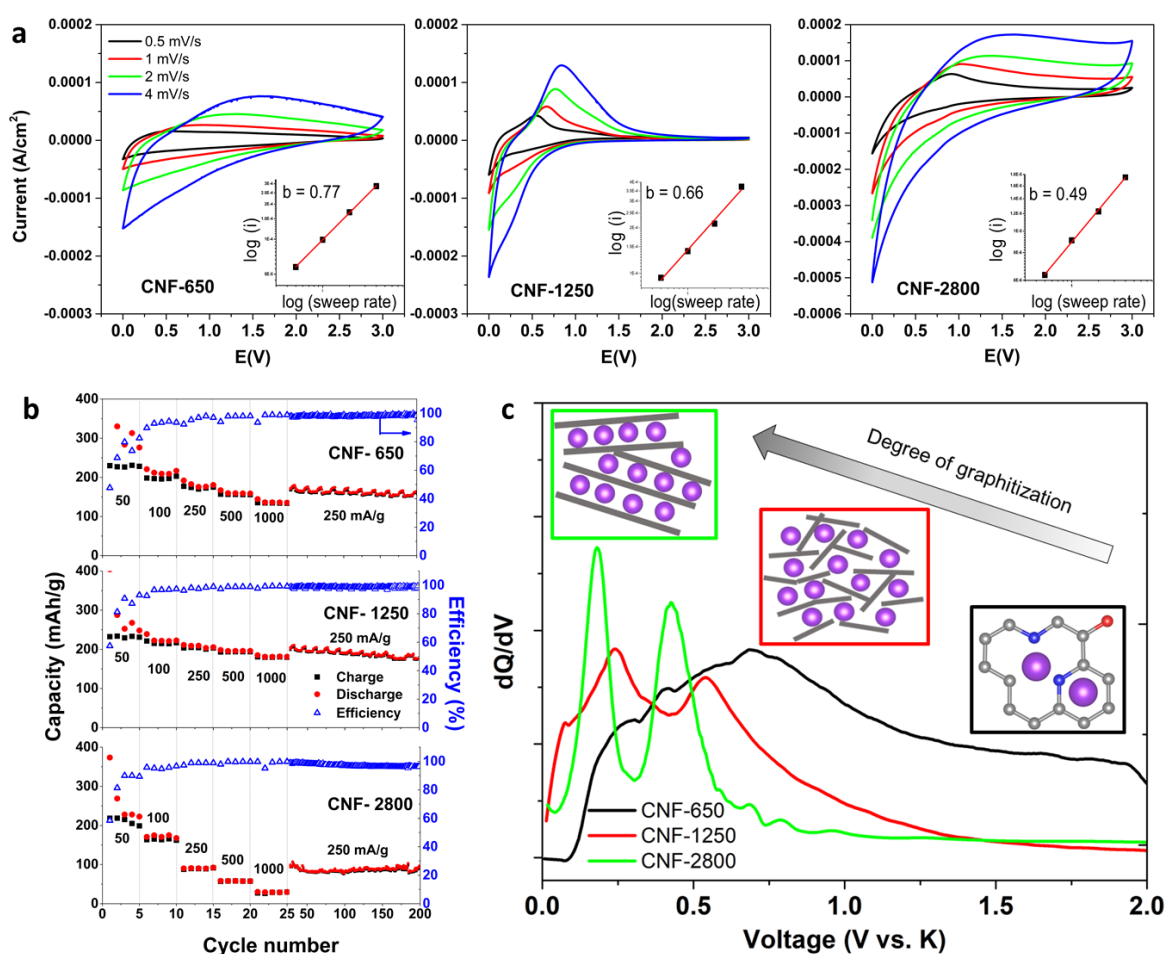

Fig. 5 Correlation between the microstructure and potassium ion storage. (a) Voltammetric responses for CNFs at sweep rates 0.5, 1, 2 and 4 mV/s, the inset is fitting of the voltammetric sweep data using Eq. 2. (b) Rate capability and cyclic performance of CNF films at current densities ranging from 50 to 1000 mA/g. (c) dQ/dV curves of CNF films at the oxidation. The inset shows the illustrations of main K-ion storage mechanism in three different regions.

The above results affirm the close correlation between the microstructure of carbon materials and their K ion storage behaviours. Depending on the atomic structure, three dominant mechanisms are proposed in carbon materials: i) Low temperature carbonized sample has a disordered structure accompanied with considerate amounts of heteroatoms like N and O. Uptake of K ions mainly occurs through reactions with the defects and functional groups, which take place at high potentials of over 0.5 V; ii) A mediate temperature between 1000 and 2000 °C produces partially ordered carbon with few layers of graphene sheets, which act as active sites for the adsorption of K ions at ~0.5 V; and iii) Highly graphitized carbon through annealing at above 2000 °C possesses remarkable graphitic domains, enabling the intercalation of K ions at an average potential of 0.25 V. The presence of various mechanisms is summarized in Fig. 5c, which helps to design advanced carbon anodes by introducing additional active sites. Previously, a reversible capacity of 240~280 mAh/g has been reported for graphitic, porous and mesoporous carbon [8,13-16]. Here, a reversible capacity around 280 mAh/g at 20 mA/g is obtained for CNFs which is among the highest values ever reported.

A question required to answer before adopting the active sites is their rate capability and reversibility towards long-term cycling. The structural stability of the materials is primarily affected by charge storage sites, which will also bring about the difference in charge transfer kinetics. The rate capability and cyclic performance of CNFs are thus tested and compared in Fig. 5b. The initial capacities of the CNFs at a current density of 50 mA/g are similar, i.e., around 220 mAh/g, suggesting the equal-capability of the active sites in uptaking K ions. The capacity gradual decreased with increasing current densities, and the CNF-1250 delivers the best capacity retention among the three samples. For instance, at a high current of 1000 mA/g, a capacity of ~180 mAh/g remains in CNF-1250 accounting for 77% of its capacity at 50 mA/g. In comparison, only ~134 and ~29 mAh/g is left in CNF-650 and CNF-2800, respectively. The rate performance is governed by both the electronic conductivity and ionic diffusion rate. The electronic conductivity of CNFs is mainly influenced by the carbonization temperature, whereas a high annealing temperature will significantly increase the electronic conductivity. A four-order improvement in the value is found when the temperature increases from 650 (10^{-4} S/cm) to 1250 °C (5.4 S/cm), explaining the better rate performance of CNF-1250. The electronic conductivity is further increased to 27.4 S/cm when the temperature goes to 2800 °C. Nevertheless, CNF-2800 does not show a good performance at a high current rate, which is attributed to the lower

K-ion diffusivity (D) arising from higher activation energy for intercalation behavior than adsorption (see discussion below). It may be improved by dilating the d-spacing as widely adopted in Na-ion batteries [35]. As discussed before, storage of K ions in CNF-650 and CNF-1250 mainly makes use of the adsorption which is a surface reaction rather than intercalation in the bulk material. It is not surprising that surface behavior shows less rate dependence. Fortunately, the intercalation does not destroy the carbon structures, which is reflected in the long-term cyclic stability for 200 cycles. A substantial volume change of 60% would occur if stage-I GIC KC_8 is formed, it is a delight to find this partially graphitized carbon is able to maintain its structural stability upon repeated insertion/extraction, capacity retention of 94.5% is delivered after 200 cycles for CNF-2800. Besides, CNF-650 and CNF-1250 also show excellent cyclic stability. The capacity is recovered when the current density reduces to 250 mA/g and a satisfying capacity retention of 96.6% and 94.2% is delivered after 200 cycles for CNF-650 and CNF-1250. It suggests the large radius of K ions does not deteriorate the cyclic stability, making it possible to build long-life K-ion batteries. As a proof, the morphology of all the three types of CNFs is well preserved after 50 charge/discharge cycles (Fig. S13), confirming the stability of the microstructure upon repeated K ion insertion/extraction.

3.3   The temperature-dependence behavior of various active sites

A general concern about the batteries relying on large radius ions is the sluggish kinetics, especially at a low temperature. Understanding the temperature-dependence of each active site is essential in designing K-ion batteries for broad working temperature range. The electrochemical performance of the CNFs at 0, 25, and 50 °C is plotted in Fig. 6a, which was obtained by discharging and charging the cell at the same current density of 25 mA/g. It is found that the capacity of the CNFs decreases with lowering of the temperature. A significant drop in capacity is observed when temperature decrease to 0 °C, which is most prominent for CNF-2800. Only 60.8% of its capacity at 25 °C is maintained when the temperature goes down to 0 °C, compared to 75.2% and 79.7% for those of CNF-650 and CNF-1250. The D value at various temperature is therefore calculated to identify the ion diffusion at the electrode/electrolyte interface using electrochemical impedance spectroscopy (EIS) method (Fig. 6c) [36], and the Nyquist plots of the cells at different temperature are shown in Fig. S14. The diffusion coefficient can be calculated from the slope of the imaginary resistance and the inverse square root of angular speed in the low frequency range. The D values of CNF-650 and CNF-1250 are similar but

higher than that of CNF-2800 in all temperatures, revealing the faster kinetics of adsorption than intercalation. In addition, Nyquist analysis of the EIS spectra of the three-electrode cell (Fig. S15 and Table S1) reveals the highest charge transfer resistance for CNF-2800. Generally, the diffusivity at reaction potential under different temperatures can be plotted versus *1/kT* by the Arrhenius equation:

$$\ln D = \ln D_0 - E_a/kT \tag{3}$$

where k is the Boltzmann constant; T is the absolute temperature; D_0 is the pre-exponential factor; and the slope of the Arrhenius plot is the activation energy E_a. As shown in Fig. 6d, the activation energy is 1.165, 1.143 and 1.331 eV for CNF-650, CNF-1250 and CNF-2800, respectively. With higher activation energy, CNF-2800 is more sensitive to the temperature change than CNF-650 and 1250. In view of this, hard carbon with partially disordered structure is more feasible for the applications working at the wide temperature environment.
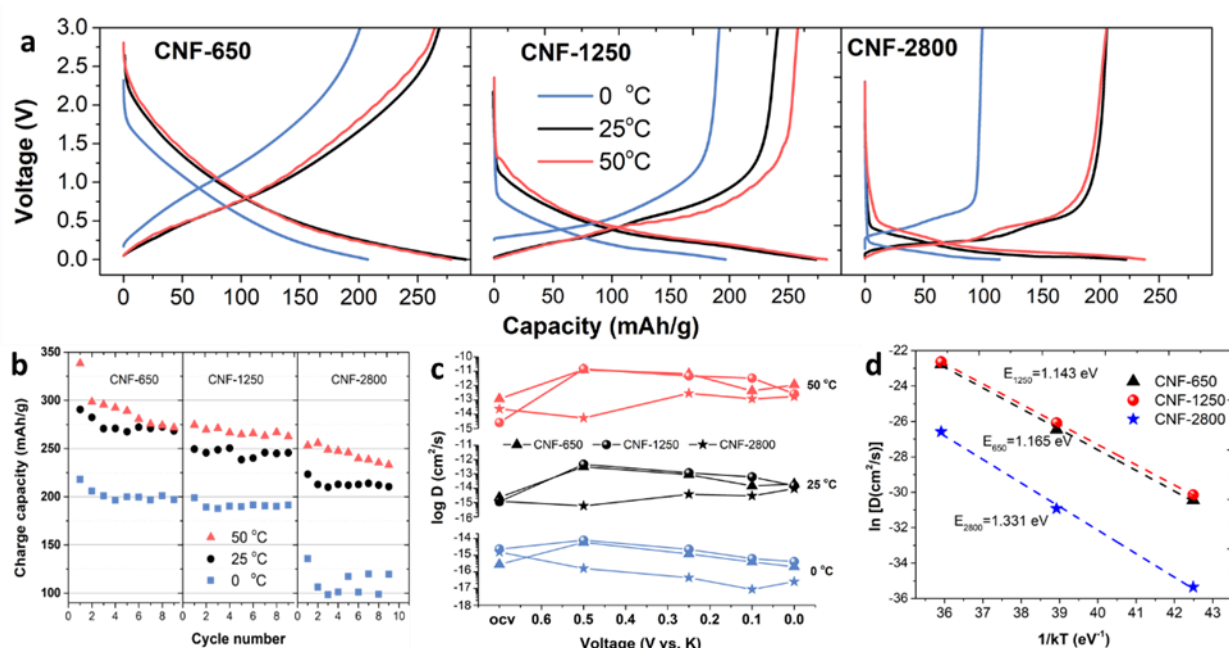

Fig. 6 Temperature-dependence behavior. (a) Voltage profile, (b) cyclic performance and (c) diffusivity of K-ion of CNFs under different temperatures. (d) Arrhenius plot of the diffusivity as a function of 1/kT for CNFs.

4. Conclusions

Using PAN-derived CNFs as model materials, we conduct a systematic study to unveil the K

ion storage behavior in carbon materials. Several active sites have been discovered, including binding with defects and functional groups, adsorption in isolated graphene sheets and intercalation in graphitic domains. The difference in ion storage mechanism leads to the variation in the voltage profiles. The intercalation of K ions in graphitic carbon mainly takes place at a voltage below 0.5 V, which will be beneficial to the battery voltage in a full cell for high energy density. The heteroatom-doped carbon provides plenty of defects for uptaking K ions at a high voltage higher than 0.5 V. Although the high potential will somehow decrease the energy density when matching with a cathode, it avoids the possible plating of K metal for safety purpose. A mediate carbonization temperature of 1250 °C results in the partly ordered carbon with randomly located graphene sheets. Both experimental and simulation results suggest that the adsorption of K ions on the surface occurs at around 0.5 V, which balances the cell voltage and safety. Furthermore, the adsorption shows fast kinetics for high power density and broad-range temperature tolerance. The capacity contribution of each site and K-ion storage mechanisms strongly depend on the atomic structure of carbon. The findings emphasize the importance of carbon microstructure design for tailoring the voltage profiles and achieving high capacity through the rationally utilizations of various active sites.

Acknowledgements

References

[1]   D. Larcher, J. Tarascon, Towards greener and more sustainable batteries for electrical energy storage, Nat. Chem. 7 (2014) 19–29. doi:10.1038/nchem.2085.

[2]   D. Kundu, E. Talaie, V. Duffort, L.F. Nazar, The Emerging Chemistry of Sodium Ion Batteries for Electrochemical Energy Storage, Angew. Chemie Int. Ed. 54 (2015) 3431–3448. doi:10.1002/anie.201410376.

[3]   X. Wu, D.P. Leonard, X. Ji, Emerging Non-Aqueous Potassium-Ion Batteries: Challenges and Opportunities, Chem. Mater. 29 (2017) 5031–5042. doi:10.1021/acs.chemmater.7b01764.

[4]   L. Xue, Y. Li, H. Gao, W. Zhou, X. Lü, W. Kaveevivitchai, A. Manthiram, J.B. Goodenough, Low-Cost High-Energy Potassium Cathode, J. Am. Chem. Soc. 139 (2017)

2164–2167. doi:10.1021/jacs.6b12598.

[5]   X. Bie, K. Kubota, T. Hosaka, K. Chihara, S. Komaba, A novel K-ion battery: hexacyanoferrate(ii)/graphite cell, J. Mater. Chem. A Mater. Energy Sustain. 5 (2017) 4325–4330. doi:10.1039/C7TA00220C.

[6]   X. Wang, X. Xu, C. Niu, J. Meng, M. Huang, X. Liu, Z. Liu, L. Mai, Earth Abundant Fe/Mn-Based Layered Oxide Interconnected Nanowires for Advanced K-Ion Full Batteries, Nano Lett. 17 (2017) 544–550. doi:10.1021/acs.nanolett.6b04611.

[7]   K. Chihara, A. Katogi, K. Kubota, S. Komaba, KVPO $_4$ F and KVOPO $_4$ toward 4 volt-class potassium-ion batteries, Chem. Commun. 53 (2017) 5208–5211. doi:10.1039/C6CC10280H.

[8]   Z. Jian, W. Luo, X. Ji, Carbon Electrodes for K-Ion Batteries, J. Am. Chem. Soc. 137 (2015) 11566–11569. doi:10.1021/jacs.5b06809.

[9]   W. Luo, J. Wan, B. Ozdemir, W. Bao, Y. Chen, J. Dai, H. Lin, Y. Xu, F. Gu, V. Barone, L. Hu, Potassium Ion Batteries with Graphitic Materials, Nano Lett. 15 (2015) 7671–7677. doi:10.1021/acs.nanolett.5b03667.

[10] S. Komaba, T. Hasegawa, M. Dahbi, K. Kubota, Potassium intercalation into graphite to realize high-voltage/high-power potassium-ion batteries and potassium-ion capacitors, Electrochem. Commun. 60 (2015) 172–175. doi:10.1016/j.elecom.2015.09.002.

[11] T. Jin, H. Li, Y. Li, L. Jiao, J. Chen, Intercalation pseudocapacitance in flexible and self-standing V 2 O 3 porous nanofibers for high-rate and ultra-stable K ion storage, Nano Energy. 50 (2018) 462–467. doi:10.1016/j.nanoen.2018.05.056.

[12] J. Xu, Y. Dou, Z. Wei, J. Ma, Y. Deng, Y. Li, H. Liu, S. Dou, Recent Progress in Graphite Intercalation Compounds for Rechargeable Metal (Li, Na, K, Al)-Ion Batteries, Adv. Sci. 4 (2017) 1700146. doi:10.1002/advs.201700146.

[13] J. Zhao, X. Zou, Y. Zhu, Y. Xu, C. Wang, Electrochemical Intercalation of Potassium into Graphite, Adv. Funct. Mater. 26 (2016) 8103–8110. doi:10.1002/adfm.201602248.

[14] J. Yang, Z. Ju, Y. Jiang, Z. Xing, B. Xi, J. Feng, S. Xiong, Enhanced Capacity and Rate Capability of Nitrogen/Oxygen Dual-Doped Hard Carbon in Capacitive Potassium-Ion Storage, Adv. Mater. 30 (2018) 1700104. doi:10.1002/adma.201700104.

[15] Z. Jian, S. Hwang, Z. Li, A.S. Hernandez, X. Wang, Z. Xing, D. Su, X. Ji, Hard–Soft Composite Carbon as a Long-Cycling and High-Rate Anode for Potassium-Ion Batteries, Adv. Funct. Mater. 27 (2017) 1–6. doi:10.1002/adfm.201700324.

[16] W. Wang, J. Zhou, Z. Wang, L. Zhao, P. Li, Y. Yang, C. Yang, H. Huang, S. Guo, Short-Range Order in Mesoporous Carbon Boosts Potassium-Ion Battery Performance, Adv. Energy Mater. 8 (2017) 1701648. doi:10.1002/aenm.201701648.

[17] K. Share, A.P. Cohn, R. Carter, B. Rogers, C.L. Pint, Role of Nitrogen-Doped Graphene for Improved High-Capacity Potassium Ion Battery Anodes, ACS Nano. 10 (2016) 9738–9744.

doi:10.1021/acsnano.6b05998.

[18] E.M. Lotfabad, J. Ding, K. Cui, A. Kohandehghan, W.P. Kalisvaart, M. Hazelton, D. Mitlin, High-density sodium and lithium ion battery anodes from banana peels, ACS Nano. 8 (2014) 7115–7129. doi:10.1021/nn502045y.

[19] B. Zhang, Z. Xu, Y. He, S. Abouali, M. Akbari Garakani, E. Kamali Heidari, F. Kang, J.-K. Kim, Exceptional rate performance of functionalized carbon nanofiber anodes containing nanopores created by (Fe) sacrificial catalyst, Nano Energy. 4 (2014) 88–96. doi:10.1016/j.nanoen.2013.12.011.

[20] B. Zhang, Y. Yu, Z.L. Xu, S. Abouali, M. Akbari, Y.B. He, F. Kang, J.K. Kim, Correlation between atomic structure and electrochemical performance of anodes made from electrospun carbon nanofiber films, Adv. Energy Mater. 4 (2014) 1–9. doi:10.1002/aenm.201301448.

[21] P.E. Blöchl, Projector augmented-wave method, Phys. Rev. B. 50 (1994) 17953–17979. doi:10.1103/PhysRevB.50.17953.

[22] G. Kresse, J. Furthmüller, Efficient iterative schemes for *ab initio* total-energy calculations using a plane-wave basis set, Phys. Rev. B. 54 (1996) 11169–11186. doi:10.1103/PhysRevB.54.11169.

[23] J.P. Perdew, K. Burke, M. Ernzerhof, Generalized Gradient Approximation Made Simple, Phys. Rev. Lett. 77 (1996) 3865–3868. doi:10.1103/PhysRevLett.77.3865.

[24] K.I. Bolotin, K.J. Sikes, Z. Jiang, M. Klima, G. Fudenberg, J. Hone, P. Kim, H.L. Stormer, Ultrahigh electron mobility in suspended graphene, Solid State Commun. 146 (2008) 351–355. doi:10.1016/j.ssc.2008.02.024.

[25] H. Yan, N.K. Mahanta, B. Wang, S. Wang, A.R. Abramson, M. Cakmak, Structural evolution in graphitization of nanofibers and mats from electrospun polyimide–mesophase pitch blends, Carbon N. Y. 71 (2014) 303–318. doi:10.1016/j.carbon.2014.01.057.

[26] B. Zhang, C.M. Ghimbeu, C. Laberty, C. Vix-Guterl, J.M. Tarascon, Correlation between Microstructure and Na Storage Behavior in Hard Carbon, Adv. Energy Mater. 6 (2016) 1–9. doi:10.1002/aenm.201501588.

[27] S.W. Lee, N. Yabuuchi, B.M. Gallant, S. Chen, B.-S. Kim, P.T. Hammond, Y. Shao-Horn, High-power lithium batteries from functionalized carbon-nanotube electrodes, Nat. Nanotechnol. 5 (2010) 531–537. doi:10.1038/nnano.2010.116.

[28] H. Chen, M. Armand, G. Demailly, F. Dolhem, P. Poizot, J.-M. Tarascon, From Biomass to a Renewable LiXC6O6 Organic Electrode for Sustainable Li-Ion Batteries, ChemSusChem. 1 (2008) 348–355. doi:10.1002/cssc.200700161.

[29] D.A. Stevens, J.R. Dahn, High Capacity Anode Materials for Rechargeable Sodium-Ion Batteries, J. Electrochem. Soc. 147 (2000) 1271. doi:10.1149/1.1393348.

[30] J.C. Chacón-Torres, L. Wirtz, T. Pichler, Manifestation of charged and strained graphene

layers in the Raman response of graphite intercalation compounds, ACS Nano. 7 (2013) 9249–9259. doi:10.1021/nn403885k.

[31] E. Markevich, V. Baranchugov, G. Salitra, D. Aurbach, M.A. Schmidt, Behavior of Graphite Electrodes in Solutions Based on Ionic Liquids in In Situ Raman Studies, J. Electrochem. Soc. 155 (2008) A132. doi:10.1149/1.2811897.

[32] C. Sole, N.E. Drewett, L.J. Hardwick, *In situ* Raman study of lithium-ion intercalation into microcrystalline graphite, Faraday Discuss. 172 (2014) 223–237. doi:10.1039/C4FD00079J.

[33] K. Share, A.P. Cohn, R.E. Carter, C.L. Pint, Mechanism of potassium ion intercalation staging in few layered graphene from in situ Raman spectroscopy, Nanoscale. 8 (2016) 16435–16439. doi:10.1039/C6NR04084E.

[34] J.C. Chacón-Torres, S. Dzsaber, S.M. Vega-Diaz, J. Akbarzadeh, H. Peterlik, J. Kotakoski, G. Argentero, J.C. Meyer, T. Pichler, F. Simon, M. Terrones, S. Reich, Potassium intercalated multiwalled carbon nanotubes, Carbon 105 (2016) 90–95. doi:10.1016/j.carbon.2016.04.016.

[35] Z. Li, C. Bommier, Z.S. Chong, Z. Jian, T.W. Surta, X. Wang, Z. Xing, J.C. Neuefeind, W.F. Stickle, M. Dolgos, P.A. Greaney, X. Ji, Mechanism of Na-Ion Storage in Hard Carbon Anodes Revealed by Heteroatom Doping, Adv. Energy Mater. 7 (2017) 1602894. doi:10.1002/aenm.201602894.

[36] P. Yu, B.N. Popov, J.A. Ritter, R.E. White, Determination of the Lithium Ion Diffusion Coefficient in Graphite, J. Electrochem. Soc. 146 (1999) 8. doi:10.1149/1.1391556.